Article

Thermal Management System of the UNICARagil Vehicles— A Comprehensive Overview

Daniel Gehringer [1,*], Timo Kuthada [2] and Andreas Wagner [1]

1 Institute of Automotive Engineering (IFS), University of Stuttgart, Pfaffenwaldring 12, 70569 Stuttgart, Germany
2 Research Institute for Automotive Engineering and Powertrain Systems Stuttgart (FKFS), Pfaffenwaldring 12, 70569 Stuttgart, Germany
* Correspondence: daniel.gehringer@ifs.uni-stuttgart.de

Abstract: The collaboration project UNICARagil aiming to develop new autonomous battery electric vehicle concepts has progressed and the four vehicle prototypes have been built up. All seven universities and six industrial partners have worked towards this milestone. At the time of writing the four vehicles are operational and can be driven by a safety driver using a sidestick. The automated driving functions are being applied on the test track and first demonstrations are carried out. This paper gives an overview of the results, which have been achieved within the work package of the thermal onboard network. The thermal management system including the heating, ventilation and air conditioning system and its development process is explained in detail. Furthermore, climate chamber measurements with prototype hardware of a sensor data processing computer and the integration of the air conditioning control unit into the vehicle's automotive service-oriented architecture framework are described. A coupled simulation approach to predict occupant thermal comfort in one vehicle variant is presented. Simulation results using environmental conditions typical for a European summer show a comfortable environment for all six occupants. In addition, the simulation and development process of a thermoelectric heat pump is shown. First measurement results with the heat pump on a test bench are highlighted which show an achievable coefficient of performance greater than two.

Keywords: thermal management; HVAC; thermal comfort; thermoelectric heat pump

1. Introduction

The mobility behavior and therefore requirements for the development of on-road vehicles have changed. Megatrends such as autonomous driving, electrification, urbanization, big data and ridesharing pose new challenges for the automotive industry [1–3]. Many large cities today face issues such as high local emissions caused by internal combustion engines and long traffic jams during rush hours, which in turn further increase emissions [4]. Electrification of the drivetrain, as well as automation of traffic, are only two efforts made to cope with these issues. To keep up with the aforementioned developments, a consortium of seven German universities as well as six industrial partners have initiated a cooperation project named UNICARagil. The project's goal is to develop four fully autonomous battery electric vehicles (BEVs), each tailored for a different use case [5]. After the initial concept phase of the project, the driving platforms were manufactured and delivered in late 2019, which kicked off the integration of hardware into the prototypes [6]. The modular system architecture in all domains is a key focus of the project. This allows each vehicle function to serve different use cases [7], which include a: privately owned vehicle, taxi, shuttle supplementing public transportation and package delivery vehicle. The vehicles are named autoELF, autoTAXI, autoSHUTTLE and autoCARGO. By scaling up length and height of the private and taxi vehicle platform, the shuttle and cargo are made possible. The project is divided into different work packages. All results described in this paper belong

to the thermal onboard network work package, which lies within the responsibility of the Institute of Automotive Engineering (IFS) at the University of Stuttgart. The thermal onboard network includes all cooling of E/E components, drive units as well as interior air conditioning to ensure the thermal comfort of passengers.

In a previous paper [8], the planned thermal management system for the UNICARagil vehicles as well as the accompanying challenges were presented. The vehicle concepts in UNICARagil require new approaches in the field of thermal management. The use of wheel hub drives and steering actuators on all four wheels means that an inherently more complex cooling system is required than in conventional vehicles with just one engine. The vehicles operate on a 48 V voltage level supplied by four main batteries integrated into the underbody. The automated driving functions require high computing power, which is provided by the four sensor module data processing units (DPU) and the cerebrum. Computationally intensive algorithms are used to generate the environment models [9,10], which run even when the vehicle is stationary where cooling airflow is sparse. High waste heat is generated at a relatively low-temperature level. The cooling of these computing units is critical to safety, as the automated driving function can no longer be ensured if the components derate or fail due to overheating. For this reason, an independent cooling circuit for the sensitive computing hardware is provided. The second cooling circuit contains the wheel hub drives as well as their power electronics and steering actuators. Each cooling circuit is independent and can be operated separately from the other.

The use cases envisage the deployment of vehicles in urban environments, meaning that the expected average driving speed will be low. Thus, the cooling package has to be equipped with powerful fans to guarantee the safe operation of the vehicle in warm climates. The vehicles will spend a significant amount of time standing still with their large doors opened to allow entry and egress of passengers. This puts a high load on the implemented heating, ventilation and air conditioning (HVAC) system due to a high air exchange rate when relying solely on direct air heating or cooling. In winter conditions, the range of a conventional BEV can be reduced by as much as 45% through the auxiliary load needed to heat the cabin [11]. This energy demand can be limited by using air recirculation, reduction in target interior temperature, efficient use of waste heat as well as a heat pump [12,13]. These measures have been implemented in the developed vehicles and will be presented in this article. A one-box design is used for the overall shape of the vehicle body. This leads to a large interior volume and glass surfaces, which demand a powerful HVAC system to keep the cabin climate in the desired range. A typical vehicle cabin has an interior volume of around 3 m^3 [14], whereas the concept pursued in UNICARagil yields an expected volume of approximately 6.34 m^3 in the small and over 10 m^3 for the large vehicles. This large interior space and the low doorsills with a level floor throughout the vehicle also imply an unconventional package. Contrary to a conventional vehicle concept, for example, there is no transmission tunnel. A conventional driver workplace is not required; therefore, the placement and orientation of the passengers are being reconsidered [15,16]. Each of the three passenger vehicle designs will therefore have an individual interior seating concept, which in turn affects the placement and design of air vents, for instance.

This paper will give an overview of the implemented cooling and HVAC system integrated into the vehicle prototypes and the thermoelectric heat pump developed within the scope of the UNICARagil project. The thermal management system is designed to operate in ambient temperatures between 0 and 30 °C, with a solar load of up to 800 W/m^2 and no precipitation. These boundary conditions were defined in the concept phase of the project to allow for the safe operation of the automated vehicle prototypes.

2. Thermal Management System

After the concept phase and procurement of components for the thermal management system, the integration into the first driving platform of the autoCARGO began in the first quarter of 2020. In the following, the thermal management system will be divided into the cooling system and the HVAC system. Cooling all E/E components in the vehicles is critical

to safe vehicle operation, whereas the HVAC system mainly improves occupant thermal comfort. In conventional vehicles, the HVAC system also contributes to safety by keeping the driver alert and preventing windows from fogging up. In an autonomous vehicle, these functions play a subordinate role. Therefore, the first steps were the implementation of the cooling circuit for E/E components to allow downstream work packages to integrate and test their hardware. During the development of the cooling system, 0D/1D simulations using GT SUITE with different possible component combinations were carried out. The final thermal management system topology that found its way into all four vehicle prototypes is depicted in Figure 1. It comprises two separate coolant circuits with different temperature levels and a refrigerant circuit for cabin air conditioning. One circuit is managing the dynamic modules (DM) and the other circuit manages the DPUs, cerebrum as well as cabin heating. Each coolant circuit consists of a pump, cooling pack and electronic control unit (ECU). Each cooling pack comprises a heat exchanger fitted with two fans in a pull configuration. Two small fans were chosen due to packaging requirements and limited space in the wheelhouse. They are necessary to maintain cooling capacity during a standstill, which is expected to account for a non-negligible proportion of the planned use cases.
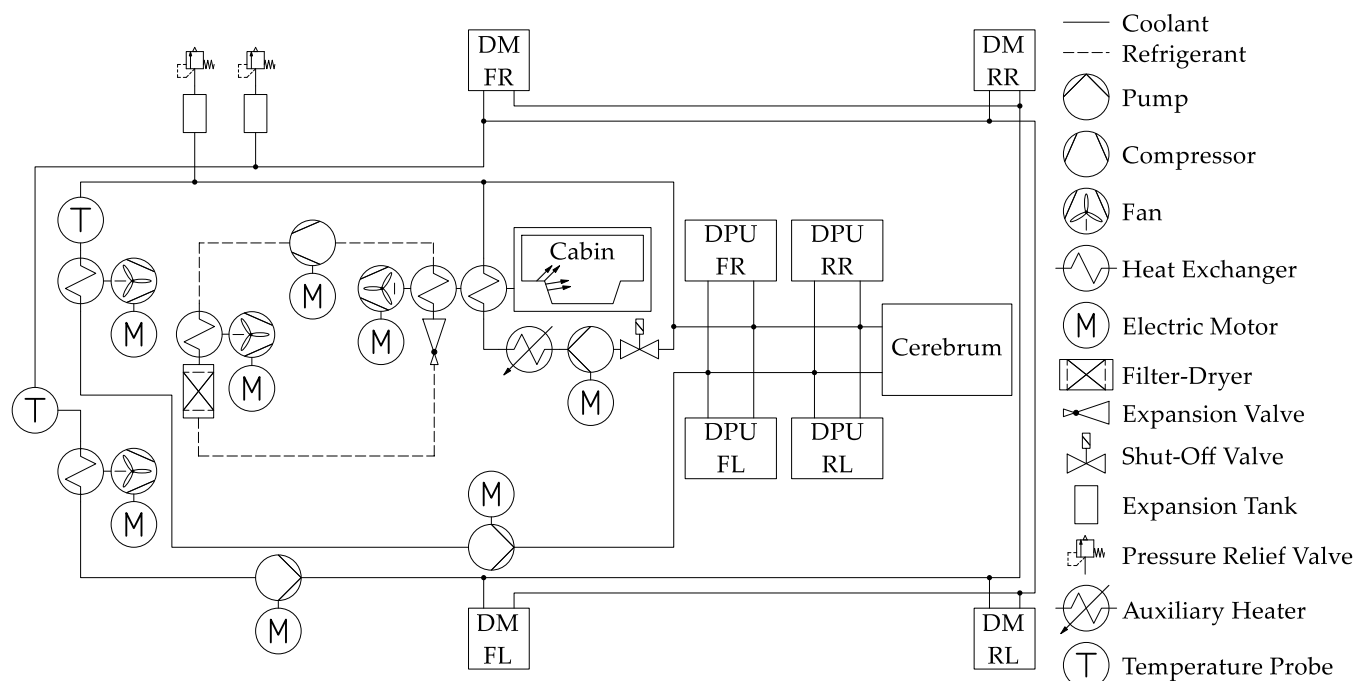

Figure 1. Implemented thermal management system topology in UNICARagil.

Preliminary testing has shown that the data processing units require a much lower cooling inlet temperature than the dynamics modules. All data processing units are situated in the low-temperature circuit due to the potential derating at cooling inlet temperatures above 53 °C. This effect will be discussed in more detail in the next section. By using liquid-cooled components in the data processing units, their excess heat can be used to heat the cabin. Each DPU outputs a peak power of 1.2 kW of which around 750 W are retrieved via the coolant loop and can be potentially used for cabin heating. This approach was chosen because the data processing units are always running during vehicle operation and the heat output is independent of the driving condition. The dynamic modules on the other hand may supply a very low amount of heat depending on vehicle speed, gradient or load. An additional electric heating element was integrated to further heat the cooling liquid on cold days before entering the cabin heat exchanger. Underfloor heating will also be integrated into the vehicles once the cabin interiors are installed in a later stage of the project.

To cool down the cabin, a refrigerant circuit with a 48 V compressor and modular HVAC-Box with several controllable air inlets and outlets was used. This modularity allows the system to adapt to each of the four different interior concepts. Inlets for cabin ventilation are situated in different locations depending on the vehicle interior concept. By the use of flexible air ducts, the HVAC system allows for a high degree of freedom in positioning the inlets for interior designers. All thermal management components had to be fitted into a package space in the vehicle's front end. Figure 2 shows the large vehicle variant of the autoSHUTTLE with all cooling and HVAC components highlighted in the right part of the picture. The vehicles use four dynamic modules in total, which each consists of a drive unit within the wheel, an inverter as well as a steering actuator. Therefore, cooling lines have to be routed throughout the vehicle and to every wheel. Both radiators and the climate condenser are mounted on the cross beam in front of the platform. The air supply is provided by the inlet opening in the lower part of the bumper.
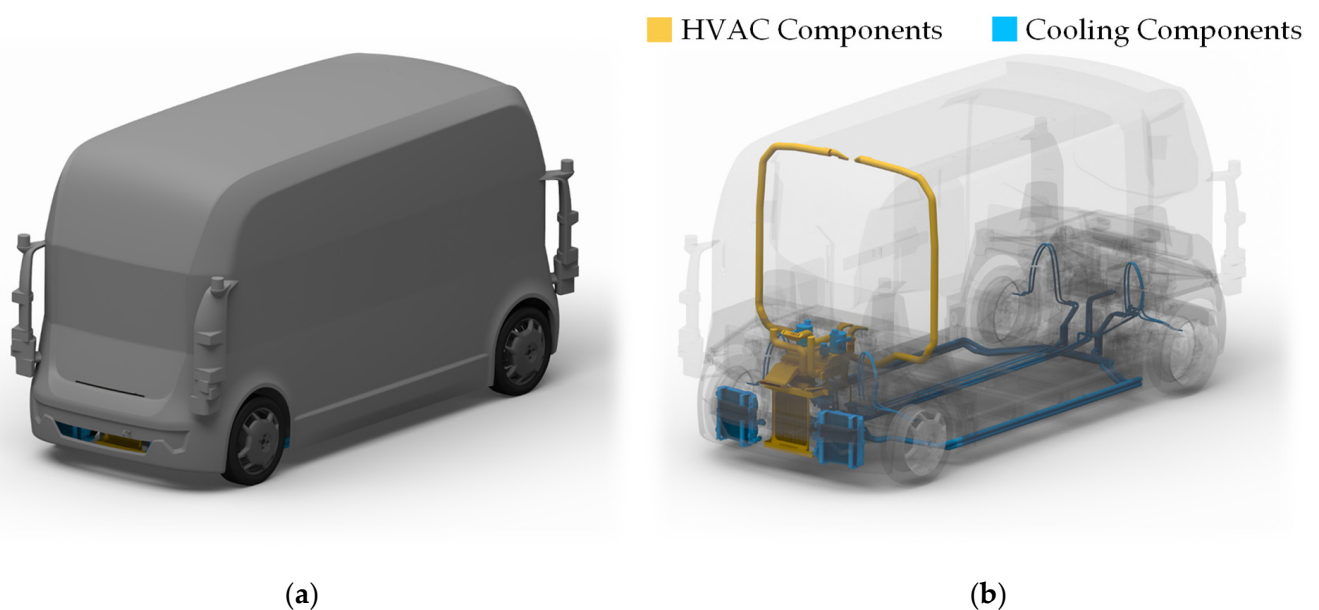

(a)　　　　**(b)**

Figure 2. (**a**) Isometric view of the large vehicle variant (autoSHUTTLE); (**b**) vehicle package with HVAC and cooling components highlighted.

The autoSHUTTLE concept shown in Figure 2 features two air conditioning inlets on the roof lining, two on the front dash in chest height and one facing the front window as defrost outlet. The two recirculating air intakes are situated on the dash beside the defrost inlet. Further details of the HVAC system are described in Section 2.2.

2.1. Thermal Testing of Sensor Module DPU

In [8], the test results of an air-cooled prototype DPU were shown. It was concluded that air-cooling is not sufficient and liquid cooling is necessary to prevent the derating of the processor clock. In the final DPU design, the processor as well as the two graphics processing unit (GPU) cards in each DPU are therefore liquid cooled while two fans on the enclosure cool all other components. Further derating tests with the final version of a DPU were carried out. To quantify the derating of the processor the quotient of current and nominal clock speed is calculated, called relative clock speed in the following. Derating is defined as the relative clock speed falling below a value of one. During the tests, the DPU was put inside a climate test chamber at a constant air temperature while the cooling liquid inlet temperature was raised, and the hardware's system load was increased to 100% using synthetic benchmarks to simulate data processing during vehicle operation. The test was carried out at 30, 40 and 50 °C test chamber temperatures, with a prior thermal soak duration of one hour. These temperatures should account for worst-case scenarios

with vehicle operation under solar load in summer months, where the compartments containing the DPUs might heat up above ambient temperature due to limited airflow. Results show that the ambient air temperature has a negligible influence on the processor clock. The main influence is the cooling liquid inlet temperature and the presence of fans in the DPU enclosure. Figure 3 shows the test results at 50 °C chamber temperature with and without a fan mounted on the enclosure of the DPU. Measurements were carried out using thermocouples type K with tolerance class one and an accuracy of ±1.5 °C. Above 53 °C cooling inlet temperature, the processor clock falls below the rated clock speed. In the test case without cooling fans in the DPU enclosure, the processor clock derated faster and at only 44 °C cooling inlet temperature. Looking into further measurement data not shown in the diagram, this can be attributed to the absence of forced convection on the power delivery components of the processor on the mainboard, which is not liquid-cooled.
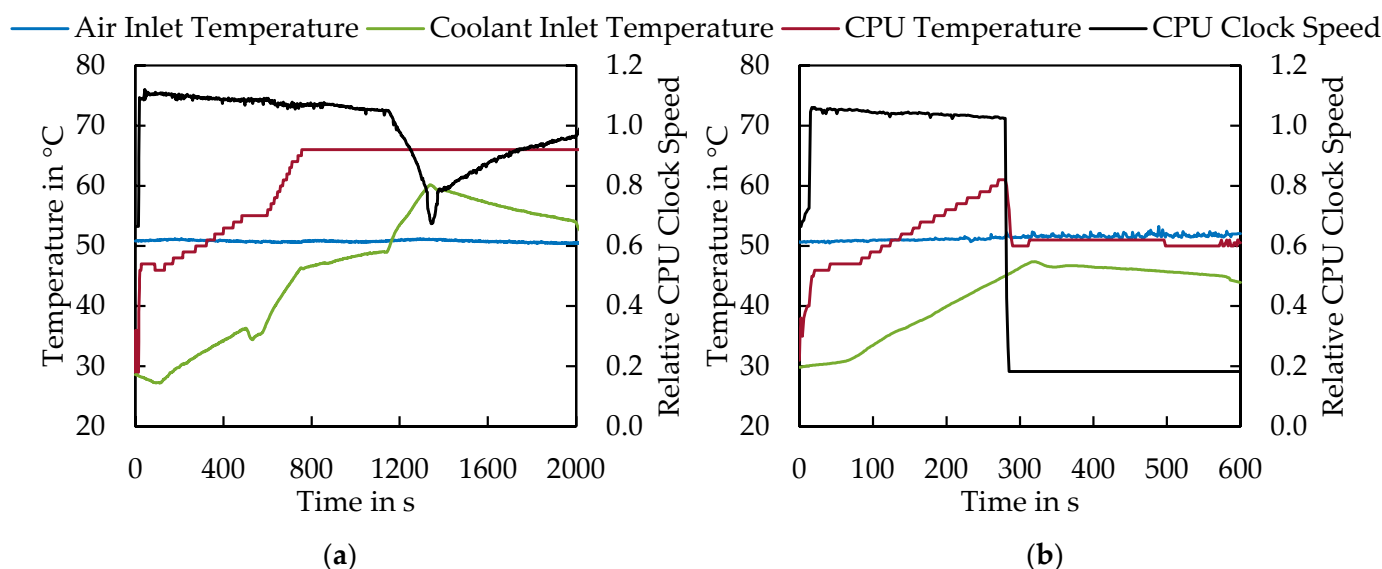

Figure 3. Thermal testing of the DPU at 50 °C test chamber temperature: (**a**) with case fans; (**b**) without case fans.

Test results described above were used to validate the DPU cooling strategy employed and tune the target temperature of the coolant loop ECU. The ECU regulates the pump speed between 25 and 100% depending on the cooling liquid temperature. The fans on the cooling pack are activated at 5 K above the target temperature of 50 °C. This temperature is measured at the cooling pack inlet and the return line of the DPUs, respectively, which can be compared in Figure 1. In measurements conducted with the DPUs, a temperature difference of 5 to 10 K between the coolant inlet and outlet can be observed depending on pump speed. This means that a target temperature of 50 °C and fan activation temperature of 55 °C measured at the coolant outlet side of the DPUs ensures a coolant inlet temperature of below 50 °C and therefore avoids derating the processor clock. This was validated during vehicle operation with sensor data processing algorithms running.

2.2. HVAC System and Control Unit

Interior air conditioning and thus thermal occupant comfort was also an important research field when developing the thermal management system. Each of the four vehicle variants has an individual interior concept. In addition to the air conditioning approach using direct air heating or cooling, surface heating is also used. The operating profile of conventional vehicles with a driver's workstation has a high proportion of time spent stationary and parked. If a vehicle is used for commuting, for example, it spends long periods parked between journeys. Here, extreme temperatures are reached in the vehicle cabin, especially in the winter and summer months. A significant portion of the air conditioning

power is used for initial heating or cooling and reaching the desired comfort temperature in the interior. The use cases of the different vehicle configurations in UNICARagil enable new operating strategies for thermal management. For example, over-conditioning of the interior during charging without passengers and the use of weather data from the cloud are feasible.

The installed HVAC box supports recirculating and fresh air modes as well as three individually controllable zones for air outlets. Seven air outlets are used to ventilate the cabin. Two are routed to the middle of the dashboard, two to the sides of the cabin, two to the headliner and one to the front window as a defrost outlet. Five inlets, of which three are used as fresh air and two as recirculation inlets, manage air supply to the HVAC box. The fresh air inlet is recessed beneath the front window, to avoid direct forced flow and water ingress into the inlet while driving. All nozzles for air intakes or outlets are adapted to the respective interior of the four different vehicles. To save energy, the recirculating mode is primarily used and the cabin air is constantly monitored using a carbon dioxide (CO_2) as well as a relative humidity sensor to efficiently control the fresh air mode. At CO_2 concentrations above 1300 ppm or relative humidity of over 65%, the fresh air mode will be activated. These pose the recommended limits in a vehicle cabin according to [14,17]. A second sensor in the cabin air intake detects total volatile organic compounds (tVOC), CO_2 equivalent, relative humidity and temperature of the intake air. These sensor signals also influence the recirculation mode state, but CO_2 concentration and relative humidity of the cabin air are always the prioritized targets in the control strategy. The control unit for managing the HVAC system has been developed; it allows the support of the ASOA framework. By this, the AC control unit can communicate with other services in the vehicle. The current interior and exterior temperatures measured by the AC control unit for example are provided as a service and can be used by other control units in the vehicle. In addition, services such as the interior human–machine interface (HMI) can influence the parameters of interior climate control if needed. A Linux operation system allows execution of the ASOA framework and services which are needed to communicate with other services and ECUs in the vehicle. For further details on the concept of ASOA and its implementation in the UNICARagil vehicles refer to [18] and [19]. The HVAC-ECU comprises a low-power open-source single-board computer with a special-purpose expansion board and required connector interfaces. It collects all HVAC sensor data and controls the components to regulate the interior climate and air quality. Figure 4 shows an input-output model of the climate control unit with associated actuators and sensors. The ECU shown in the middle is divided into four main functions: sensor data acquisition, fuzzy controller, output signal generation and climate control ASOA service [20]. The arrows in the diagram indicate data flow between components or functions. The first function reads and evaluates the sensor data. It then provides the sensor data to the climate control ASOA service and fuzzy controller. The fuzzy controller determines the appropriate actuator strategy based on the supplied sensor data and constraints provided by the climate control ASOA service. The last function converts the controller output data into a suitable actuator signal for the HVAC components. The climate control ASOA service can publish the received sensor data via Ethernet to other services in the vehicle network and can receive constraints such as target interior temperature or control curve which it then supplies to the fuzzy controller. The sensors and actuators can be clustered into different subgroups. Input sensor data are shown on the left and actuated hardware is on the right side of the diagram.
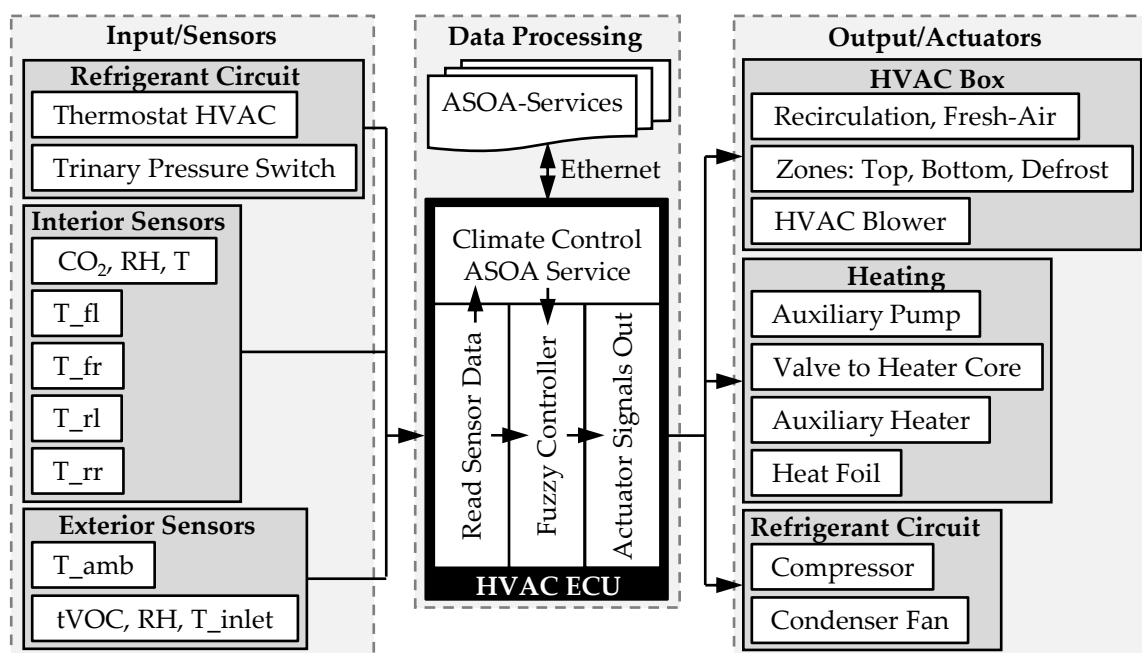
Figure 4. Input-output model of the HVAC-System ECU.

If no target interior temperature is received from other services via the ASOA framework, it is calculated depending on the current ambient temperature. There are two possible calculation rules: Normal and Eco. In Normal mode, the interior temperature is calculated in accordance with DIN 1946-3:2006-07 [21]. In Eco mode, the calculation is based on the Association of German Transport Companies (VDV) Eco Curve, which is used in service buses with short travel distances and therefore short lengths of stay for passengers [22,23]. These boundary conditions are met in the autoSHUTTLE or autoTAXI use case. The Eco curve is also suitable for the autoCARGO, where no passengers are present in the vehicle during autonomous delivery operation. With this Eco curve, energy can be conserved in extreme climates while taking weather-adapted clothing of occupants as well as the length of stay into account. A comparison between the two implemented control curves is shown in Figure 5. The curve selection can be influenced via the climate control service and ASOA framework, so the vehicle controller can decide if thermal comfort or driving range is of higher importance depending on current boundary conditions such as remaining energy or planned route.
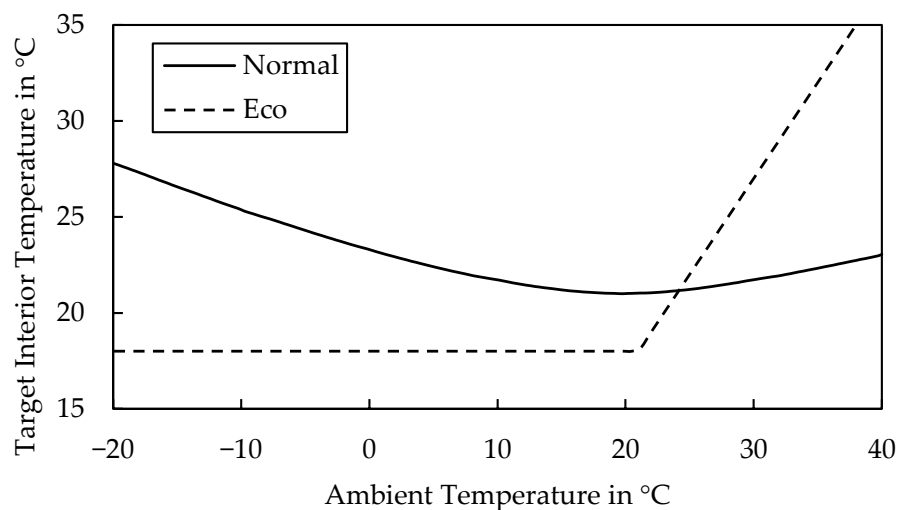

Figure 5. Target interior temperature curves used by the controller, based on [21–23].

The HVAC control unit case comprises all input/output connectors. The extension board comprises several motor drivers, relays and a DC/DC converter [24]. The DC/DC converter on the board is used to supply power to the development board, all hardware on the extension board, sensors, as well as the switching contacts of external relays used to actuate the HVAC components. This way the 12 V level available in the vehicles can be used to directly power the ECU and its components. Temperatures are measured using negative temperature coefficient (NTC) sensors with an accuracy of $\pm 0.5\,°C$. The sensors for CO_2 concentration in the interior and tVOC concentration of exterior air communicate via an inter-integrated circuit (I^2C) bus. For safety reasons a trinary pressure switch integrated into the refrigerant circuit monitors pressure and can deactivate the compressor via a hardware override in case of abnormal pressure rise. In addition, activation of the condenser fan is controlled using the signal of the trinary switch at a medium pressure level. A thermostat fitted within the HVAC box is used to regulate the compressor speed based on the temperature between the fins of the evaporator to avoid icing and in consequence potential damage to the evaporator core. The HVAC blower is controlled using a DC voltage output in the range of 0 to 5 V supplied to a pulse-width modulation (PWM) signal generator. Air distribution is achieved using five servomotors on the HVAC box. Heating components such as the auxiliary heater or heat foil are actuated using external 12 V relays.

3. Simulation of Thermal Cabin Comfort

After finishing the design phase computer-aided design (CAD) geometry of the vehicle, interior and all components were available and a cabin model for the thermal cabin comfort was set up. A coupled simulation approach using the software PowerFLOW and PowerTHERM was chosen. This allows thermal comfort evaluation using a comfort model. The following section will highlight the model built and some key results for a summer simulation case. The flow field in the passenger compartment is calculated using a CFD simulation, which passes the near-wall fluid temperatures and heat transfer coefficients to the thermal solver. The thermal solver calculates the surface temperatures of the parts and returns them to the CFD solver, this process is repeated until a steady state is reached. A simulation approach is needed because the integration of the interiors is scheduled at the project end and the vehicle prototypes are used for implementation of the automation functions on the proving ground, so measurements in the real vehicle with the final interiors are not possible during the project. The CAD geometry was prepared and discretized to be used in the simulation environment. For the cabin, all relevant interior surfaces of the model are retained and a closed volume is created. Parts that are not in direct contact with the interior flow are removed to reduce simulation effort. The thickness and material layers of the cabin walls are modeled in the thermal solver. The autoSHUTTLE has the largest interior volume ($10.75\ m^3$), the largest exterior surfaces and window areas and is designed for six occupants. This represents the most challenging case of all vehicle variants for interior air conditioning. Figure 6 shows the cabin model and the air conditioning inlets on the headliner, front interior surface and windshield of the autoSHUTTLE. All inlets are modeled with an upstream inlet section on the HVAC box to obtain a realistic flow distribution and profile in the ducting.
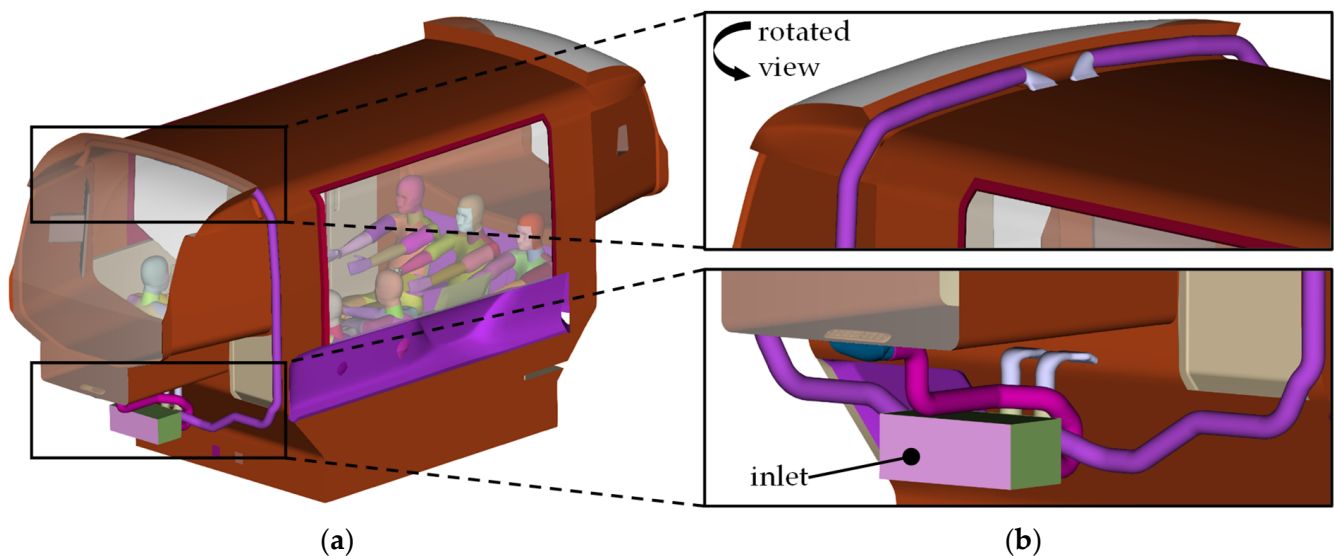
Figure 6. AutoSHUTTLE cabin simulation model: (**a**) isometric view of the model with six manikins with colored segments; (**b**) HVAC box with inlet and ducting.

The simulation model of the autoELF is based on an analogous design and only differs in size, the interior concept as well as positioning of the air inlets. The interior volume of this smaller vehicle is 6.34 m^3. Heat exchange with the environment as well as the influence of solar radiation is modeled in the thermal solver. For this purpose, the interior surfaces of the cabin are virtually thickened and provided with layers of different materials. The vehicle hardware prototype was used as a source for material types and layer thicknesses. Human models in the autoSHUTTLE occupy all six seats. In the autoELF, four human models are used according to the seating configuration of the vehicle. All human models are divided into individual segments in order to evaluate the comfort sensation on different parts of the body, as shown in Figure 6. The models are built up in several layers and have thermoregulatory mechanisms to reproduce the heat exchange with the environment simulating blood flow, sweat, respiration and skin evaporation; the modeling approach is based on the Berkeley comfort model [25,26].

Simulation cases include a winter case with 0 °C ambient temperature and a summer case with 30 °C ambient temperature and 800 W/m^2 solar loads on the vehicle roof. These simulations were carried out with different inlet mass flows and temperatures. Initial boundary conditions were defined to correspond to a preconditioned cabin. All Human models are set up with a sedentary activity type and 1.2 met activity level, which corresponds to a metabolic rate of 70 W/m^2 [27]. The clothing of the manikins is modeled via additional material layers above the skin and is adapted according to the simulated boundary conditions. Simulation results of the summer case with the autoSHUTTLE geometry are illustrated in Figure 7. Results show the sensation and comfort of all six occupants, which are individually colored. The Berkeley comfort model rates thermal sensation as well as comfort on a scale of −4 to 4 for individual body parts as well as the whole body [26]. On the sensation scale, −4 means very cold, 0 neutral and 4 very hot sensations perceived by the occupant [28]. On the comfort scale, −4 means that occupants feel very uncomfortable and 4 means they feel very comfortable [29]. Whole body sensation and comfort values are calculated based on [30]. The simulation results show good overall comfort and sensation. All comfort ratings for the different seating positions are similar and there are no outliers with larger deviations. Most body parts show a neutral sensation and a good comfort rating. Only the arms indicate a slightly warm sensation and lower comfort. This can be attributed to the missing air outlet at the passenger shoulder level and the solar radiation transmitted through the side glass. Most airflow is directed to the lower

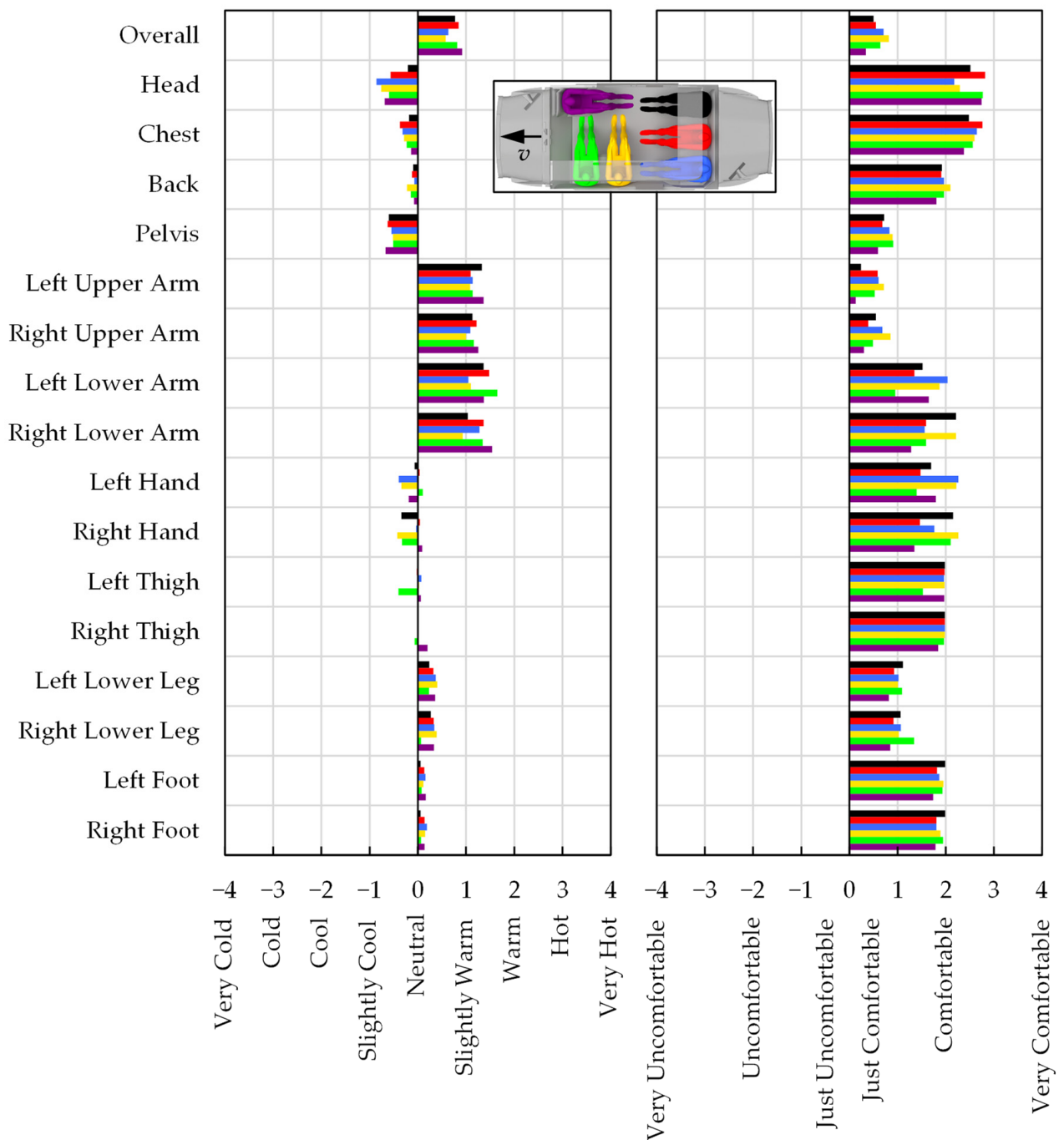part of the cabin by the lower outlets and the upper part by the outlets on the headliner of the vehicle.

Figure 7. Simulated thermal sensation and comfort results of all occupants in the summer case.

The developed model can be used over the further course of the project for tuning the air conditioning system of the vehicles under different boundary conditions. This way, operating conditions and their influence on the thermal comfort of the occupants can be estimated even without the use of a functional prototype. After integration of the vehicle interiors, measurements with a thermal comfort manikin are planned to validate the simulation approach and further asses the passenger comfort during real-world vehicle operation.

4. Thermoelectric Heat Pump

Thermoelectric modules (TEM) are used in many technical fields either as power generators or in heat pump applications [31]. A two-stage thermoelectric heat pump was developed as part of the project to make efficient use of the waste heat from data processing units and drive units. The heat pump makes it possible to raise the waste heat from the drive unit and DPU cooling circuits to a higher temperature level and thus make it usable for heating the passenger compartment. Here, significantly higher efficiencies are achieved than with positive temperature coefficient (PTC) auxiliary heaters commonly used in electric vehicles [32]. By exploiting the thermoelectric effect and using doped semiconductor elements, the heat pump requires no moving parts. Potentially harmful refrigerants and the associated maintenance can also be eliminated. The thermoelectric effect provides heat transport as a function of current flow and the charge carriers that move with it. Electrons moving through an electrical conductor transport energy. Electrons with higher energy contribute more to the current flow, thus the transported energy can be directly influenced by the current intensity. At the transition between two materials, the energy of the electrons changes and the difference is released or absorbed as heat at the junction. Figure 8a shows a thermoelectric leg pair during heat pump operation. The semiconductors are connected with metallic contact bridges. The electrons on the n-doped side and the holes on the p-doped side move in opposite directions. Depending on the polarity, they move towards or away from the junction. This results in the heating or cooling of the junction and thus a heat transfer between the two sides of the element [33,34]. In the example considered, the cold side is at the top and the hot side is at the bottom, the heat flows from the cold side to the hot side. Peltier elements can thus be regarded in simplified terms as electric heat pumps. Commercially available TEMs consist of several hundred leg pairs, where each leg pair has a cross-section of approximately 1 mm^2. Depending on the polarity and direction of the current flow, the direction of the heat flow can be reversed. Thus heating, as well as cooling of a component, can be realized. The temperature differences achieved between hot and cold sides in commercially available elements are in the range of 50–80 K. TEMs can have varying efficiency depending on the operating point. The efficiency can be characterized by the coefficient of performance (COP), which is defined as the quotient of transported heat flow $\dot{Q}_c$ and electrical power P_{el}. The COP depends on the temperature difference prevalent between the cold and hot sides as well as the electrical power. Figure 8b shows the coefficient of performance of a TEM versus the operating current for various temperature differences. It can be seen that when operating at a current close to the maximum current, the coefficient of performance and thus the efficiency decreases. TEMs can achieve COPs of over one, this means they can transport more heat between their hot and cold plates than they consume electrical energy. This is because the heat flow on the hot side results from the addition of the heat flow absorbed on the cold side and internal resistive heating effects caused by the supplied electrical power. It is also evident that as the temperature difference increases, the coefficient of performance decreases. Thus, the maximum power specified by the manufacturer can be achieved only at the temperature difference of 0 K. If the maximum possible temperature difference is reached, no more heat can be transported and a steady state condition is established. The maximum heating or cooling power at a temperature difference of 0 K, as well as the maximum achievable temperature difference, are used to characterize and select TEMs. These values, as well as the power curves depending on the current and the temperature difference, are published by the manufacturer in the data sheet of a TEM.
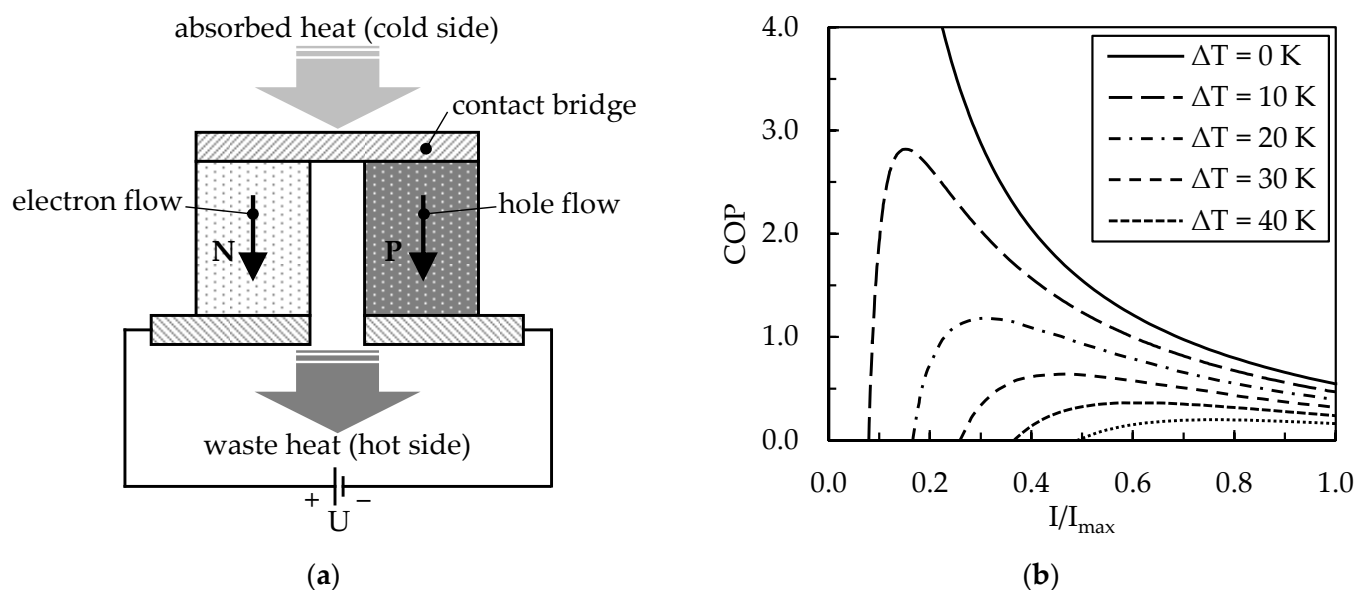
Figure 8. (**a**) Thermoelectric leg pair; (**b**) Coefficient of performance versus supply current in dependence of temperature difference [35].

The two stages of the heat pump allow for a combination of three cooling circuits with different temperature levels and coolants. All sensor module DPUs are combined in the low-temperature heat exchanger at the bottom, the middle combines all dynamic modules and inverters in the medium-temperature loop and the high-temperature loop is used to heat the cabin during winter. Splitting the temperature difference over two TEM stages decreases the temperature difference in each individual TEM, which in turn increases the efficiency. The amount of thermoelectric modules is adjusted based on the cooling requirement. Between the low and medium-temperature heat exchangers, there are six thermoelectric modules. In the upper stage, ten modules are used. The two-stage design also allows cooling of the cabin in a transitional season before or after summer if the cooling requirement of the DPU or dynamic module circuit is low. In that case, heat can be pumped from the interior circuit into the other circuits where it can then be dissipated via the main coolers of the vehicle. The performance of the heat pump can be scaled and adapted to different vehicle concepts through variations in TEM count and cooling plate size. Thus, efficient heating of small cars up to buses or shuttles is possible.

The development of the heat pump is divided into four steps. First, a 0D/1D simulation model of the heat pump was set up using GT-SUITE. The second phase consisted of the CAD design and 3D-CFD simulation of several cooling plate designs with different fluid channels. The CFD results were later looped back into the 0D/1D simulation model to increase its accuracy. This was followed by the procurement and manufacturing of all required parts. After the hardware prototype of the heat pump was built, the first measurements were carried out.

4.1. Simulation Approach

A thermal 0D/1D simulation was used to assess the required number of thermoelectric modules in each stage. The coolant circuits are simplified and the heat input of components such as the drive units or DPUs are modeled using volumes with heat inputs. The three cooling circuits are connected thermally through heat-exchanging plates and thermoelectric modules. The DPU cooling circuit is situated at the bottom and it is thermally connected to the drive unit circuit using six TEMs. The modules are connected to thermal masses representing an aluminum cooling plate, which is in turn connected to the fluid loop via a convection link. The interior heating circuit is connected in the same way using ten modules at the top of the drive unit circuit. The efficiency of thermoelectric modules is

mainly dependent on the load as well as the temperature difference [35,36]. Due to the relatively high power demand for cabin heating in the UNICARagil vehicles, modules with the highest maximum cooling power available were chosen. The performance data of the chosen thermoelectric modules are listed in Table 1. These parameters were input into the simulation model.

Table 1. Performance data of the selected thermoelectric modules at $25 \pm 0.5\,^{\circ}\text{C}$ test temperature.

Property	Symbol	Value
Maximal Current	I_{max}	28 A
Maximal Voltage	U_{max}	27.7 V
Maximal Temperature Difference	ΔT_{max}	66 K
Maximal Cooling Power	$Q_{c,max}$	430 W
Resistance	R_{AC}	0.87 Ω

To assess different cooling plate designs, a CFD simulation approach with coupled thermal solver was used. In total, 20 different plate designs were simulated. The cooling channel designs were mainly influenced by the requirement to manufacture the plates on a milling machine. This part of development overlapped with the CAD design process; therefore, an iterative approach with manufacturability in mind was chosen. First, different cooling channel geometries were simulated and compared to a baseline simulation with an empty cooling channel with a rectangular flow cross-section. The best version was then chosen for detail optimization. To quantify the quality of heat transfer the convection heat flux in the cooling channels is used to compare different designs. The pressure drop between the inlet and outlet of the cooling plate is also considered. The Nusselt number is used to quantify the ratio of convective and conductive heat transfer between a fluid and a solid at the boundary. It is defined as

$$Nu = \frac{\alpha l}{\lambda}, \tag{1}$$

where α is the heat transfer coefficient, l is the characteristic length and λ is the thermal conductivity [37]. To assess the pressure drop of different designs the dimensionless pressure coefficient is calculated as

$$c_p = \frac{p_x - p_\infty}{\frac{\rho}{2} \cdot w_\infty^2}, \tag{2}$$

using the pressure difference between undisturbed flow p_∞ and plate flow p_x, coolant density ρ and undisturbed flow speed w_∞ [38]. Figure 9 shows the final detail optimization process with four cooling plate versions. The convection flux of a section of the cooling channels is shown in the left part of the figure. Changes include the modification of crossbar length in order to achieve a uniform distribution of coolant after deflection as well as the insertion of blind holes to increase turbulence and thus increase boundary layer mixing. The diagram in the right part of the figure shows the dimensionless Nusselt number versus the pressure coefficient of the simulated versions. Through improved coolant distribution over the channels, the pressure loss drops when comparing cooling plate versions V1, V2 and V3. The effect of the boundary layer mixing caused by the blind holes can be seen by comparing the Nusselt number of V3 and V4, it has a negligible effect on pressure loss. V4 is the final chosen and implemented design for the heat pump.
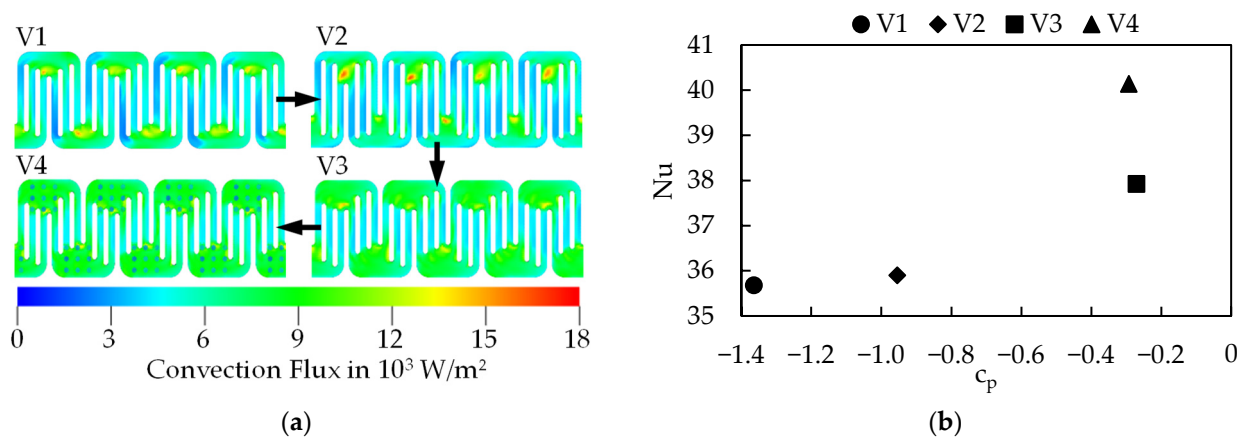
Figure 9. Final optimization of cooling plate versions: (**a**) convection flux in excerpts of the cooling plate channels; (**b**) Nusselt number over pressure coefficient. Based on [39].

4.2. Design and Manufacturing

All cooling plates of the different stages have the same channel design. Figure 10 shows an exploded view of the cabin cooling plate on the left and the complete thermoelectric heat pump assembly on the right. The cabin cooling plate is rotated and situated at the bottom in the right part of the figure. The main dimensions of the heat pump are 425 mm × 200 mm × 118 mm. The Inlet and outlet fittings of the cooling plates have a diameter of 19 mm. The upper stage between the dynamic module and data processing unit loop has six TEMs with a total power of 2.58 kW. The lower stage between the dynamic module and cabin loop has ten TEMs with a total power of 4.3 kW. Refer to Table 1 for performance data of the used TEM. In each stage, two TEMs are electrically connected in series and these pairs are then connected in parallel. This allows for the use of 48 V onboard voltage from the traction batteries in the vehicles.
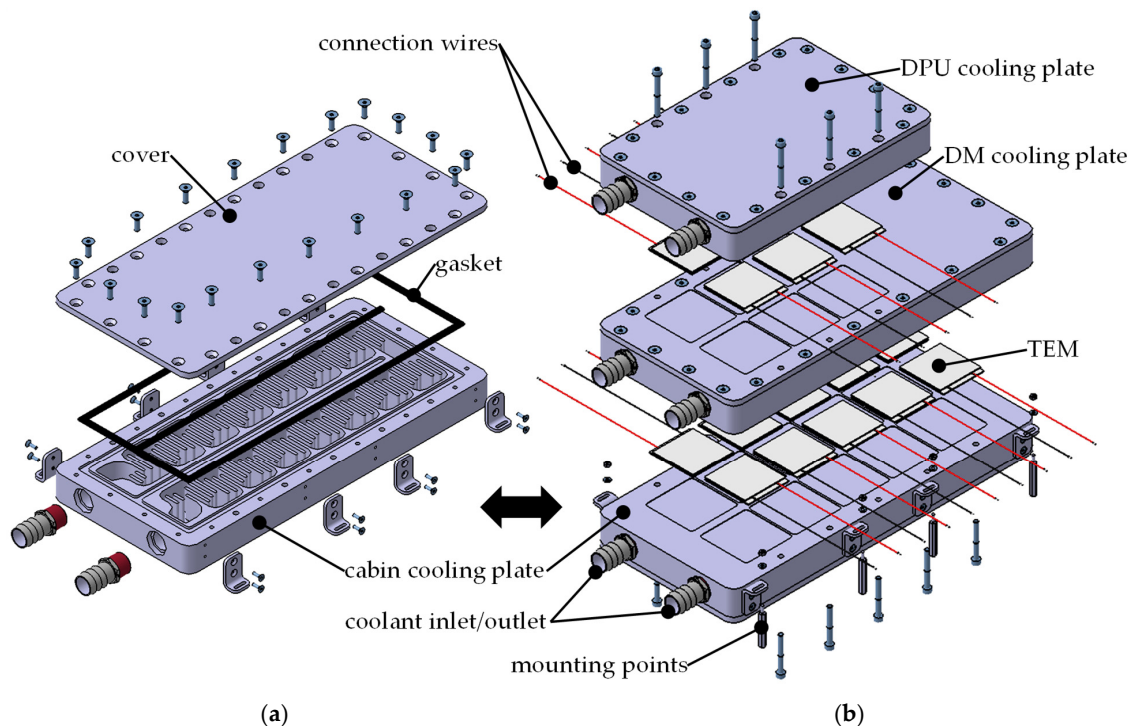

Figure 10. Exploded view of the thermoelectric heat pump: (**a**) Cabin cooling plate with final coolant channel design; (**b**) Complete assembly with all three cooling plates and TEMs.

Each plate consists of the main plate with the coolant channels and a top cover. To prevent leakage, a gasket with a rectangular cross-section is used around the perimeter of the plate. A second gasket on the central divider between the inlet and outlet side prevents a cross flow and mixing of coolant before the deflection curve at the end of the plate. The gaskets are situated in a groove on the main plate. Several screws ensure uniform pressure on the gasket. A detailed calculation of the bolt connection, in accordance with [40] and [41], was carried out taking into account coolant pressure, pre-deformation of the gasket, loss of pretension force as well as plate and screw deformation. Hose fittings with a self-sealing thread are used to connect each cooling plate to the corresponding cooling circuit. The TEMs are mounted between the cooling plates and the electrical connection wires are routed out via the sides of the assembly. Small rectangular recesses are milled into the bottom of the plates and covers to ensure the correct positioning of the TEMs. The top and bottom plates are mounted to the plate in the middle using longer screws from the top and bottom. Thermal contact resistance between two solid bodies is influenced by the contact pressure [42], this means the highest contact pressure possible is pursued to enhance heat transfer. However, the maximal contact pressure allowed is prescribed by the strength of the TEMs. This required a second bolt calculation for the second row of screws connecting the plates to each other and taking the maximal allowed contact pressure into account. These screws are arranged in such a way that the connecting line between two screws runs through the centerline of two TEMs. This ensures an even pressure distribution, which avoids damage to the elements and improves heat exchange. Eight mounting points on the lower cooling plate allow the heat pump assembly to be fitted into the vehicle or test bench.

4.3. Measurements and Results

After the manufacturing of components, a test stand for heat pump measurements was built. The test stand includes the heat pump, a coolant pump for each circuit, expansion tanks, flow measurement devices, thermocouples, power supplies, coolant conditioning systems and an HVAC box. Sheathed thermocouples are used to measure coolant inlet and outlet temperatures in the hoses. The heat flux exchanged through a cooling plate can then be calculated by

$$\dot{Q} = \dot{V} \cdot \rho(T) \cdot \Delta T \cdot c_p(T), \tag{3}$$

with the coolants volumetric flow rate $\dot{V}$, the temperature difference between inlet and outlet ΔT as well as temperature-dependent density $\rho(T)$ and specific heat capacity of the coolant $c_p(T)$. Density and heat capacity are determined using the averaged coolant temperature and literature values [37]. The electric power consumed by the TEMs is determined by measuring the supply voltage and current of the connected power supply. With these two values, the COP of each stage can be calculated. The DPU cooling plate is supplied with a coolant flow of 520 l/h and 40 °C. The connected conditioning system supplies a constant 3.8 kW heat input to simulate the four DPUs and cerebrum in the vehicle. The second conditioning system supplies up to 4 kW heat input with a temperature level of 60 °C to simulate the drive units and inverters, the volume flow is also 520 l/h. All measurements were carried out over a time of ten minutes. The interior heating circuit is operated at a temperature level of 80 °C. Two scenarios were investigated, one with pre-conditioned coolant circuits to simulate the vehicle during operation and one with coolant at ambient temperature to account for a potential heat-up phase. Measurements were taken at three different supply current ratios of 0.15, 0.3 and 0.45 of I/I_{max}. The HVAC blower rotational speed was varied in three steps: lowest possible speed, medium and maximum possible speed. Measurement results are shown in Figure 11, the diagrams show the resulting COP over available heating power exerted via the interior heat exchanger. The pre-heated coolant leads to a higher COP and heating power. At current levels of 0.15, the COP is at or slightly above 2. With higher supply currents, the COP falls rapidly to a value of below 1. The HVAC blower speed mainly affects the heat rate transferred to the air via the interior heat exchanger in the HVAC box. COP and usable heat rate rise with

rising blower speed, although in most cases it is approximately the same at medium and high speeds. Only at a supply current ratio of 0.45, a difference between medium and high blower speed levels can be observed.
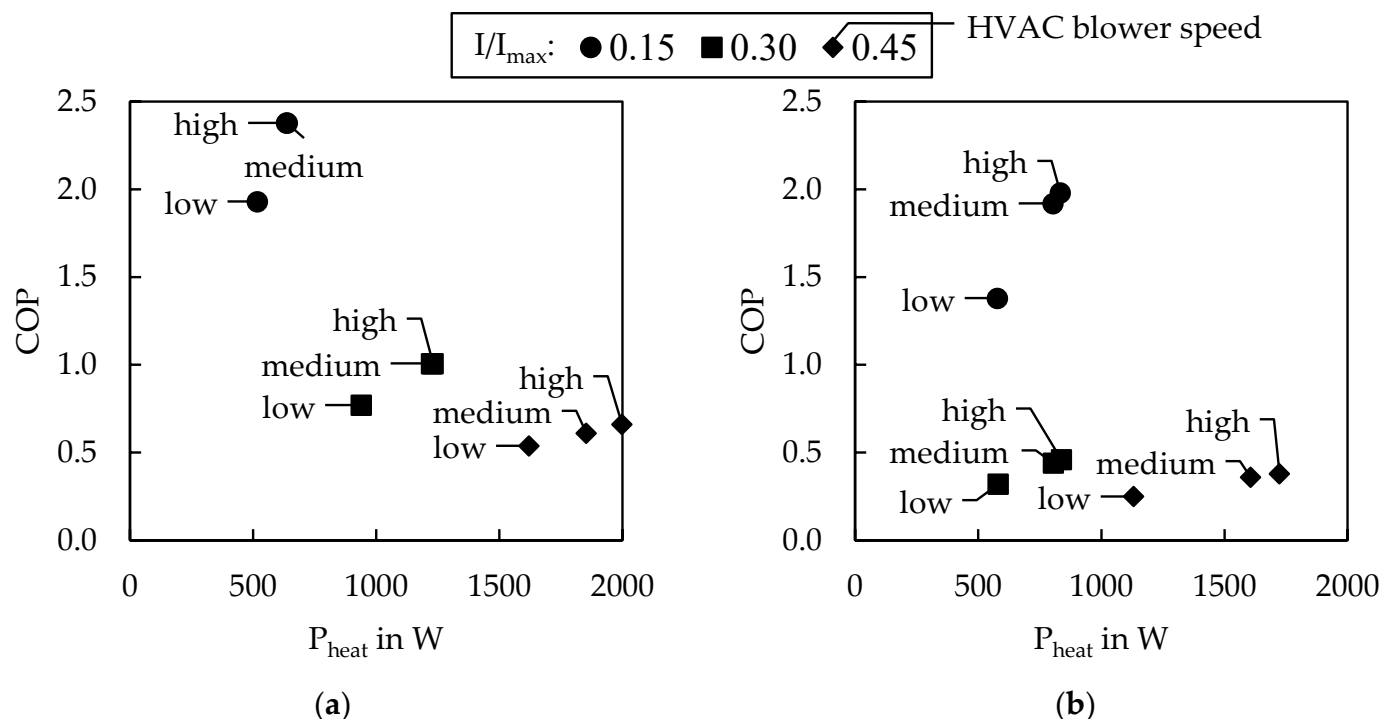

Figure 11. Measurement results showing coefficient of performance over-heating power: (**a**) with pre-conditioned coolant loop; (**b**) without pre-conditioned coolant loop. Measurement results taken from [43].

Although the COPs achieved at a current ratio of 0.15 are well above 1, the usable heat rate in the cabin heat exchanger is rather low. The heat rates of 600 to 700 W would be enough for maintaining interior temperatures in a pre-heated cabin during mild winter days. Higher heat rates are possible by raising the supply current ratio but lead to a COP below 1. Each measurement was performed with a fixed voltage and current supply. Further efficiency increases could be possible using an advanced control strategy and dynamically varying the power supply depending on the required heating output. It is possible to increase efficiency by making use of thermal insulation around the heat pump and between the heat exchanger plates. The effect of such insulation measures could be evaluated in future investigations.

5. Summary and Outlook

Within the scope of the UNICARagil project a thermal management system including the HVAC system for the cabin has been developed. A key challenge was the cooling of the computational hardware needed for all autonomous driving functions, which is an integral part of a safe vehicle operation. This included intensive testing of the computer hardware under various climatic conditions in a test chamber. Results show that active air-cooling of computational hardware is not sufficient to avoid a reduction in the clock rate and therefore compromises vehicle safety. Hot spots in the packing rooms of computer hardware must be avoided because they can lead to derating even if most of the heat is dissipated by a central water cooling system. The integration of all thermal management hardware components has been completed, and the cooling circuits are successfully operating in all four vehicles. The current status of the project as well as pictures and videos of the vehicles in motion are published on the project website www.unicaragil.de (accessed on 30 November 2022).

A control unit with ASOA support for the HVAC system using various sensors efficiently controlling the interior climate was developed and implemented into the vehicles. The sensors include CO_2, humidity, and four temperature sensors in the cabin, as well as a total volatile organic compound, humidity, and two temperature sensors on the exterior of the vehicle. Through the use of these sensors an extended recirculation rate and therefore decreased load on the traction battery is achieved without compromising interior air quality. Waste heat generated as a by-product of sensor data evaluation can be used to heat the cabin and therefore increase the efficiency of the vehicles. The control unit features different curves for target interior temperature determination and can communicate with other ECUs in the vehicle via Ethernet. This allows the energy management system of the vehicles to influence the power demand of the HVAC system if needed. The next step is to fine-tune the control parameters during real-world vehicle operation.

The thermal passenger comfort has been evaluated using a coupled simulation approach between CFD and thermal solver. This was possible even though no vehicle hardware prototype was available in this development stage. Results of the large vehicle variant indicate good thermal comfort considering that this topic was not the main focus during vehicle development and design of the interior concepts. After the integration of the interiors into the vehicles, thermal comfort measurements in the vehicles can be carried out to evaluate the final vehicle comfort values and validate simulation results.

The development of a multi-stage thermoelectric heat pump has been shown. During the concept phase, the heat pump was simulated using a 0D/1D simulation model. Later a coupled simulation using CFD and a thermal solver was used to design the cooling channels in the heat pump. The CAD design process of the assembly and first measurement results on a test stand with a prototype of the heat pump was shown. The results indicate potential energy savings when compared to a state-of-the-art resistive heating element, especially during steady-state operation with low heat demand. Future steps will be to use an improved control strategy for energy supply to the thermoelectric module as well as improved insulation of the heat pump from the surrounding environment to increase its efficiency further.

In the oncoming final project phase, the interiors will be integrated into the vehicles. During this step, the interior sensors will be installed into the interior surfaces and the heating surfaces are added together with the floor assembly. This will then complete all necessary components for a fully operational HVAC system in the cars. At the project's final event, the vehicle prototypes will be demonstrated to the public.

Abbreviations

The following abbreviations are used in the article.

AC	Air conditioning
ASOA	Automotive service-oriented architecture
BEV	Battery electric vehicle
CAD	Computer-aided design
CFD	Computational fluid dynamics
CO_2	Carbon dioxide
COP	Coefficient of performance
DC	Direct current
DM	Dynamic module
DPU	Data processing unit
ECU	Electronic control unit
FDM	Fused deposition modeling
GPU	Graphics processing unit
HMI	Human machine interface
HVAC	Heating, ventilation and air conditioning
I^2C	Inter-integrated circuit
IFS	Institute of Automotive Engineering
NTC	Negative temperature coefficient
PTC	Positive temperature coefficient
PWM	Pulse-width modulation
TEM	Thermoelectric module
tVOC	Total volatile organic compounds
VDV	Association of German Transport Companies

References

1. Zukunftsinstitut GmbH. *The Evolution of Mobility. A Zukunftsinstitut Study Commissioned by ADAC*; ADAC e.V.: Munich, Germany, 2017.
2. Fraedrich, E.; Kröger, L.; Bahamonde-Birke, F.; Frenzel, I.; Liedtke, G.; Trommer, S.; Lenz, B.; Heinrichs, D. *Automatisiertes Fahren im Personen und Güterverkehr. Auswirkungen auf den Modal-Split, das Verkehrssystem und Die Siedlungsstrukturen*; e-Mobil BW GmbH, Deutsches Zentrum für Luft- und Raumfahrt e.V. (DLR)—Institut für Verkehrsforschung; Ministerium für Verkehr Baden-Württemberg: Stuttgart, Germany, 2017.
3. Frieske, B.; van den Adel, B.; Schwarz-Kocher, M.; Stieler, S.; Schnabel, A.; Tözün, R. *Strukturstudie BWe Mobil 2019. Transformation Durch Elektromobilität und Perspektiven der Digitalisierung*; e-Mobil BW GmbH, Deutsches Zentrum für Luft- und Raumfahrt e.V. (DLR)—Institut für Fahrzeugkonzepte; BridgingIT GmbH: Stuttgart, Germany, 2019.
4. Cookson, G. *INRIX Global Traffic Scorecard*; INRIX Research: Kirkland, DC, USA, 2018.
5. Woopen, T.; Lampe, B.; Böddeker, T.; Eckstein, L.; Kampmann, A.; Alrifaee, B.; Kowalewski, S.; Moormann, D.; Stolte, T.; Jatzkowski, I.; et al. UNICARagil—Disruptive modular architectures for agile, automated vehicle concepts. In Proceedings of the 27th Aachen Colloquium Automobile and Engine Technology, Aachen, Germany, 8–10 October 2018. [CrossRef]
6. Woopen, T.; van Kempen, R.; Böddeker, T.; Eckstein, L. UNICARagil—Where we are and where we are going. In Proceedings of the 29th Aachen Colloquium Sustainable Mobility, Aachen, Germany, 5–7 October 2020. [CrossRef]
7. Van Kempen, R.; Woopen, T.; Eckstein, L. UNICARagil: Agile development of self-driving vehicles. In Proceedings of the 30th Aachen Colloquium Sustainable Mobility, Aachen, Germany, 4–6 October 2021. [CrossRef]
8. Gehringer, D.; Keilhoff, D.; Kuthada, T.; Wiedemann, J. UNICARagil: Challenges in thermal management for autonomous vehicle concepts. In Proceedings of the 12th FKFS Conference, Stuttgart, Germany, 1–2 October 2019.
9. Henning, M.; Muller, J.C.; Gies, F.; Buchholz, M.; Dietmayer, K. Situation-aware environment perception using a multi-layer attention map. *IEEE Trans. Intell. Veh.* **2022**. *online ahead of print*. [CrossRef]
10. Henning, M.; Buchholz, M.; Dietmayer, K. Situation-aware environment perception for decentralized automation architectures. In Proceedings of the 2022 IEEE Intelligent Vehicles Symposium (IV), Aachen, Germany, 4–9 June 2022; pp. 1087–1092. [CrossRef]
11. Chowdhury, S.; Leitzel, L.; Zima, M.; Santacesaria, M.; Titov, G.; Lustbader, J.; Rugh, J.; Winkler, J.; Khawaja, A.; Govindarajalu, M. Total thermal management of Battery Electric Vehicles (BEVs). *SAE Tech. Pap.* **2018**. [CrossRef]
12. Auer, M. *Ein Beitrag zur Erhöhung der Reichweite Eines Batterieelektrischen Fahrzeugs Durch Prädikatives Thermomanagement*, 1st ed.; Springer Vieweg: Wiesbaden, Germany, 2016. [CrossRef]
13. Pan, L.; Liu, C.; Zhang, Z.; Wang, T.; Shi, J.; Chen, J. Energy-saving effect of utilizing recirculated air in electric vehicle air conditioning system. *Int. J. Refrig.* **2019**, *102*, 122–129. [CrossRef]
14. Großmann, H. *Pkw-Klimatisierung: Physikalische Grundlagen und technische Umsetzung*, 2nd ed.; Springer Vieweg: Berlin, Germany, 2013. [CrossRef]

15. Schräder, T.; Stolte, T.; Jatzkowski, I.; Graubohm, R.; Maurer, M. An Approach for a requirement analysis for an autonomous family vehicle. In Proceedings of the 2019 IEEE Intelligent Vehicles Symposium (IV), Paris, France, 9–12 June 2019; pp. 1587–1603. [CrossRef]
16. Köhler, A.L.; Prinz, F.; Wang, L.; Becker, J.; Voß, G.M.I.; Schulte, T.; Depner, N.; Ladwig, S.; Eckstein, L. How will we travel autonomously? User needs for interior concepts and requirements towards occupant safety. In Proceedings of the 28th Aachen Colloquium Automobile and Engine Technology, Aachen, Germany, 7–9 October 2019.
17. *ANSI/ASHREA Standard 62.1-2016*; Addendum d to ANSI/ASHREA Standard 62.1-2016, Ventilation for Acceptable Indoor Air Quality. ASHRAE Special Publications: Atlanta, GA, USA, 2016.
18. Kampmann, A.; Alrifaee, B.; Kohout, M.; Wüstenberg, A.; Woopen, T.; Nolte, M.; Eckstein, L.; Kowalewski, S. A dynamic service-oriented software architecture for highly automated vehicles. In Proceedings of the IEEE Intelligent Transportation Systems Conference (ITSC), Auckland, New Zealand, 27–30 October 2019. [CrossRef]
19. Mokhtarian, A.; Kampmann, A.; Alrifaee, B.; Kowalewski, S. The dynamic service-oriented software architecture for the UNICARagil Project. In Proceedings of the 29th Aachen Colloquium Sustainable Mobility, Aachen, Germany, 5–7 October 2020. [CrossRef]
20. Strößer, B.S. *Integration und Inbetriebnahme Eines ASOA-Steuergeräts zur Regelung von Klimatisierungskomponenten*; Studienarbeit, Institut für Fahrzeugtechnik Stuttgart; Universität Stuttgart: Stuttgart, Germany, 2021.
21. *DIN 1946-3:2006-07*; Raumlufttechnik—Teil 3: Klimatisierung von Personenkraftwagen und Lastkraftwagen. Beuth Verlag GmbH: Berlin, Germany, 2006. Available online: https://www.beuth.de/de/norm/din-1946-3/87022434 (accessed on 30 November 2022).
22. Birkel, H.; Bronnenberg, P.; Krawinkel, E.; Roch, R.; Walter, K. *VDV-Schrift 236: Klimatisierung von Linienbussen der Zulassungsklassen I (Stadtbus) und II (Überlandbus), für Konventionell Angetriebene Diesel- und Gasbusse als auch für Hybrid-, Brennstoffzellen- und Elektrobusse, 11/2018*; Beka GmbH: Cologne, Germany, 2018.
23. Schmidt, H.; Classen, H.; Birkel, P.; Bronnenberg, P.; Cramer, U.; Eberwein, B.; Fendt, F.; Pütz, R. *VDV-Schrift 236/1: Life-Cycle-Cost-Optimierte Klimatisierung von Linienbussen—Teilklimatisierung Fahrgastraum—Vollklimatisierung Fahrerarbeitsplatz. 08/2009*; Beka GmbH: Cologne, Germany, 2009.
24. Wizl, J. *Entwicklung eines ASOA-Steuergeräts zur Regelung von Thermomanagementkomponenten in Autonomen Fahrzeugen*; Studienarbeit, Institut für Fahrzeugtechnik Stuttgart; Universität Stuttgart: Stuttgart, Germany, 2020.
25. Dassault Systèmes. *PowerTHERM 13.0–Human Modeling User's Guide*; Dassault Systèmes Simulia Corp.: Vélizy-Villacoublay, France, 2019.
26. Zhang, H. Human Thermal Sensation and Comfort in Transient and Non-Uniform Thermal Environments. Ph.D. Thesis, University of California, Berkeley, CA, USA, 2003.
27. *ANSI/ASHREA Standard 55-2017*; Thermal Environmental Conditions for Human Occupancy. ASHRAE Special Publications: Atlanta, GA, USA, 2017.
28. Zhang, H.; Arens, E.; Huizenga, C.; Han, T. Thermal sensation and comfort models for non-uniform and transient environments, part I: Local sensation of individual body parts. *Build. Environ.* **2010**, *45*, 380–388. [CrossRef]
29. Zhang, H.; Arens, E.; Huizenga, C.; Han, T. Thermal sensation and comfort models for non-uniform and transient environments, part II: Local comfort of individual body parts. *Build. Environ.* **2010**, *45*, 389–398. [CrossRef]
30. Zhang, H.; Arens, E.; Huizenga, C.; Han, T. Thermal sensation and comfort models for non-uniform and transient environments, part III: Whole-body sensation and comfort. *Build. Environ.* **2010**, *45*, 399–410. [CrossRef]
31. Zheng, X.F.; Liu, C.X.; Yan, Y.Y.; Wang, Q. A review of thermoelectrics research—Recent developments and potentials for sustainable and renewable energy applications. *Renew. Sustain. Energy Rev.* **2014**, *32*, 486–503. [CrossRef]
32. Neumeister, D.; Heneka, C.; Wiebelt, A. Thermoelectric heat pump for efficient cabin heating. In Proceedings of the 23rd Aachen Colloquium Automobile and Engine Technology, Aachen, Germany, 6–8 October 2014.
33. Huebener, R. *Leiter, Halbleiter, Supraleiter: Eine Kompakte Einführung in Geschichte, Entwicklung und Theorie der Festkörperphysik*, 2nd ed.; Springer Spektrum: Berlin, Germany, 2017. [CrossRef]
34. Goldsmid, J.H. *Introduction to Thermoelectricity*, 1st ed.; Springer Series in Materials Science; Springer: Berlin/Heidelberg, Germany, 2010. [CrossRef]
35. Peltier Element Design Guide. Available online: https://www.meerstetter.ch/customer-center/compendium/32-tec-peltier-element-design-guide (accessed on 17 August 2022).
36. Somdalen, R. *Untersuchung Einer Thermoelektrischen Wärmepumpe für den Einsatz in Elektrofahrzeugen. Abschlussbericht zum Forschungsvorhaben*; Technische Universität Braunschweig: Braunschweig, Germany, 2014.
37. VDI-Gesellschaft Verfahrenstechnik und Chemieingenieurwesen (GVC). *VDI-Wärmeatlas*, 11th ed.; Springer: Berlin/Heidelberg, Germany, 2013. [CrossRef]
38. Böswirth, L.; Bschorer, S. *Technische Strömungslehre, Lehr und Übungsbuch*, 10th ed.; Springer Vieweg: Wiesbaden, Germany, 2014. [CrossRef]
39. Huber, L. *Auslegung und Konstruktion Einer Thermoelektrischen Wärmepumpe*; Studienarbeit, Institut für Fahrzeugtechnik Stuttgart; Universität Stuttgart: Stuttgart, Germany, 2020.
40. Haas, W. *Grundlehrgang Dichtungstechnik*; Institut für Maschinenelemente, Bereich Dichtungstechnik, Universität Stuttgart: Stuttgart, Germany, 2014.

41. *VDI-Gesellschaft Produkt- und Prozessgestaltung (GPP) VDI 2230 Blatt 1 Systematische Berechnung Hochbeanspruchter Schraubverbindungen—Zylindrische Einschraubverbindungen*; Beuth Verlag GmbH: Berlin, Germany, 2015. Available online: https://www.beuth.de/de/technische-regel/vdi-2230-blatt-1/242566299?websource=vdin (accessed on 30 November 2022).
42. Herwig, H. *Wärmeübertragung A-Z*, 1st ed.; Springer: Berlin/Heidelberg, Germany, 2000. [CrossRef]
43. Lichtenstein, L. *Aufbau und thermische Vermessung Einer Mehrstufigen Thermoelektrischen Wärmepumpe*; Studienarbeit, Institut für Fahrzeugtechnik Stuttgart; Universität Stuttgart: Stuttgart, Germany, 2021.